Molecular BioSystems

Accepted Manuscript

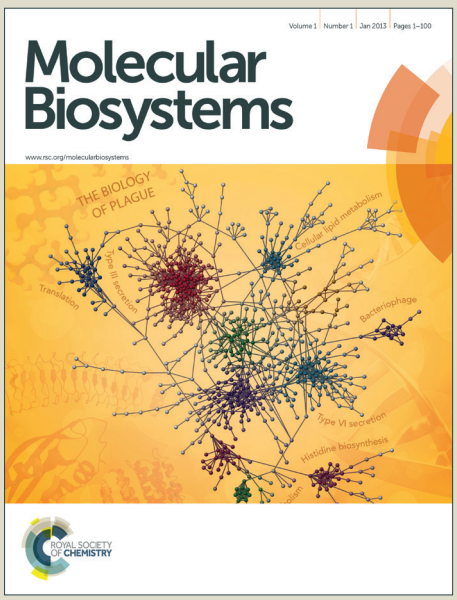

ROYAL SOCIETY OF CHEMISTRY

www.rsc.org/molecularbiosystems

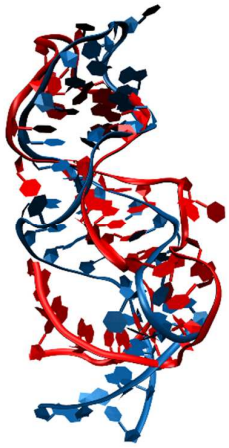

MD simulations revealed reversibility of the long ranged conformational changes of the HCV RNA subdomain IIa.

Molecular BioSystems

RSCPublishing

ARTICLE

Computational study of the IRES subdomain IIa structural plasticity and the ligand binding affinity

Cite this: DOI: 10.1039/x0xx00000x

Marina Grabar Branilović [a] and Sanja Tomić *[a]

Received 00th January 2012,
Accepted 00th January 2012

DOI: 10.1039/x0xx00000x

www.rsc.org/

The internal ribosome entry site (IRES) of the hepatitis C virus (HCV) drives noncanonical initiation of protein synthesis necessary for viral replication. In order to fulfil its role in HCV translation initiation its subdomain IIa should adopt an L-shaped conformation. However, according to the present knowledge, the bent topology of IIa would prevent the progression of the ribosome from initiation to productive translation. In order to be released from the ribosome, IIa should transform from bended to an extended form. With the purpose to study the IRES subdomain IIa plasticity and stability we performed detailed molecular dynamics (MD) simulations of the ligand free RNA and its (native and mutated) complexes with the potential HCV inhibitors. We have shown that upon ligand removal conformation of the IIa subdomain changed from an extended into the L-shaped one during several tens of ns. Differently, binding of the benzimidazole translation inhibitors locked IIa in the extended conformation. On the other hand, the newly discovered translation inhibitor diaminopiperidine (DAP), in agreement with the experimentally based assumptions, stabilized IIa RNA in the bent conformation during MD simulations. Apparently the efficient locking of the subdomain IIa in one form is one of the requirements the HCV RNA targeting drugs should fulfil.

Introduction

Hepatitis C virus (HCV) chronically infects over 160 million people worldwide.[1] Although more than 20 years passed of its discovery there is still no vaccine available and just recently two specific (protease targeting) inhibitors were approved as the first direct antiviral drugs for the treatment of HCV infection.[2] There are also several polymerase (NS5B) inhibitors which due to low fidelity of the HCV RNA-dependent polymerase (NS5B)[3-5] are effective only in the combined therapies i.e. in combination with pegylated interferon and ribavirin.[6]

Beside the regulatory proteins the other potential target for the HCV inhibitors is its RNA. Several studies have provided information about the specific viral RNA motifs that play an active role in the viral life cycle (see [7] and references therein). The regulatory motifs controlling translation and replication of the viral RNA are mostly found at the 5' and 3' untranslated regions (UTRs). In particular, viral protein synthesis is under the control of the internal ribosome entry site (IRES) element, a complex RNA structure located at the 5' UTR that hijack the cellular translation machinery.

The IRES RNA sequence is highly conserved among HCV isolates and genotypes.[8] This conservation underscores the importance of the HCV IRES RNA to the viral replication cycle and reflects the specificity of the interactions between the IRES RNA and the translation machinery. The HCV IRES consists of four domains I-IV. In solution, these elements fold into an extended tertiary structure with two major, independently folded domains, namely domain III together with its extension domain IV and domain II.[9] Domain II is organized into a basal domain IIa and an apical domain IIb, of which only domain IIb interacts with the 40S subunit.[10,11] The mutations, which disrupted base pairing in stem II abolished IRES activity and could be only partially restored by compensatory mutations.[11] On the other hand mutations of the larger domain III, abolished IRES activity, but only slightly effected the RNA binding affinity toward 40S subunit.[11]

The cryo-EM analyses of the 40S subunit and the binary HCV IRES–40S complexes revealed significant, domain II-dependent conformational changes in the 40S subunit upon IRES binding.[12,13] The interactions between the apical domain IIb and the ribosome E-site induces rotation of the ribosomal head relative to the body and the resulting opening of the mRNA entry channel latch aids to stably accommodate the HCV ORF.

Higher resolution structures of the domain II has been determined by NMR spectroscopy[14] and by X-ray diffraction on monocrystals.[15] They revealed an overall L-shape of the domain II, in agreement with previous results of the microscopic analysis[12,13] of the HCV IRES–40S complexes, suggesting that the domain II forms an independently folded module within the IRES RNA with an overall L-shape both free in solution and when bound to the 40S subunit. These findings together with the results of Filbin et al.[16] implied that L-shaped architecture of the domain II is important for the correct positioning of the viral mRNA initiation codon as well as for joining of the ribosomal subunits to form functional 80S unit.[12,16]

Dibrov et al.[17] and later on Paulsen et al.[18] showed that compounds for which it was proven that inhibit HCV replication, induced straightening of the subdomain IIa. Their finding provided a potential mechanism of these compounds to inhibit HCV replication. Further on, the authors speculated that conformational transition of the subdomain IIa from an L-shape to an extended structure may facilitate the release of domain II from the E-site to make room for deacylated tRNA during the transition to productive translation. They proposed that in natural environment such conformational change might be triggered either by interaction with a ribosomal protein or by a guanidine (G) residue wherein G could belong either to viral mRNA itself or rRNA.[19]

Already Kieff et al.[9] reported that the IRES adopted a unique three-dimensional structure at physiological salt concentrations. They showed that IRES folding is linked to magnesium uptake and is driven primarily by charge neutralization. Influence of the metal ions, Mn^{2+} and Mg^{2+} on the three dimensional structure of the IIa subdomain was studied by Dibrov et al.[17] Paulsen et al.[18] also noticed RNA stabilization upon addition of magnesium however, they found that the NMR spectra are unaffected by presence of the divalent metal cations. Within the present study we performed series of long MD simulations in order to elucidate influence of environment, mutations and ligands to the three-dimensional RNA structure plasticity and stability. We determined binding affinities for several benzimidazole compounds, translation inhibitors and an analogue, as well as for the recently characterized translation inhibitor diaminopiperidine (DAP).[19] Using QM/MM approach we determined changes in the inhibitor structure and electronic charge distribution at the presence of magnesium cations and RNA.

Materials and methods

The initial systems for our calculations were built using the three-dimensional structures of the IRES subdomain IIa determined by X-ray diffraction (34 nucleotides) (PDB ID code 3TZR)[17] and by NMR spectroscopy (38 nucleotides) (PDB ID code 2KTZ).[18] In both of them the subdomain IIa is complexed with a benzimidazole translation inhibitor **2** (Fig. 1).

Complexes with inhibitor **1** and analouge **3** were constructed from the crystallographically determined structure of the complex IIa-**2**[17] by replacing **2** (*S* enantiomer) with either **1** or **3** (in both cases the *S* enantiomer). Since by the experimental methods it was not possible to determine the ligand stereochemistry unambiguously,[17] besides with the *S* enantiomer we also simulated IIa complex with the *R* enantiomer of **2**. However, it turned out that this complex is less stable than the one with *S* enantiomer of **2**. Because of that all further simulations with benzimidazole ligands were performed using *S* enantiomers.

Additionally, the RNA-**2** complex was constructed using the L-shaped structures of the IIa subdomain, obtained by MD simulations of the ligand free RNA (structures determined by X-ray and NMR). Ligands were built and protonated using the module 'Builder' within the program INSIGHTII.[20]

We also performed molecular modelling studies for the ligand free IIa domain, native and mutated, in, and without, presence of magnesium ions. Two double mutants were constructed by exchanging the C58-G110 Watson-Crick pair with G58-C110 (mutant I) and U58-A110 pair (mutant II).

Since neither the experimentally determined structure of the HCV RNA–DAP complex has been available nor it was clear if it binds to the IIa subdomain as an intercalator or a groove binder, we built several IIa–DAP complexes using the L-shaped form of IIa obtained by MD simulations of the RNA-**3** complex. In two complexes ("bm1" and "bm2") DAP was bound to IIa as an intercalator and in one as a groove binder ("bm3"). In "bm1" and "bm2" DAP was partly intercalated between the neighbouring bases A53 and G52 of the IIa since the experiments with benzimidazole inhibitors indicated this region as the ligand binding site. In both cases, phenyl methyl ketone was intercalated and the rest of the molecule was placed in the minor groove of RNA. In the first binding mode ("bm1"), diaminopiperidine part was placed in the direction of the bent part of the L-shaped IIa and in the second binding mode ("bm2") the whole ligand was rotated for 180° so that diaminopiperidine part was pointing in the opposite direction of the IIa bent.

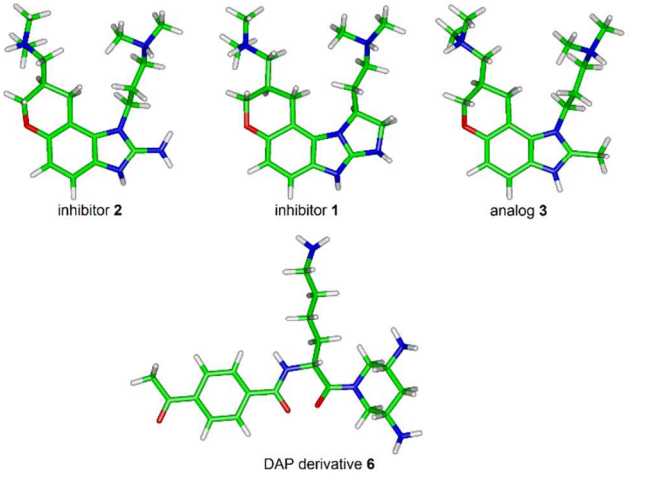

Fig. 1 Translation inhibitors. Above: benzimidazole inhibitors **1** and **2** and analogue **3**, below: diaminopiperidine derivative **6**.

The general AMBER force field GAFF[21] and AMBER ff99SB force field of Duan et al.[22] were used to parameterize systems. The partial atomic charges, required for ligands parameterization, were derived using the DFT (B3LYP/3-21G) method as implemented in the program Gaussian09.[23-25]

The xLeap module of AMBER11[26] was used to obtain topology and coordinate files for the constructed systems. Each of the complexes and the free ds-RNAs were placed in the octahedral box filled with TIP3P type water molecules. A water buffer of 8 Å was used. Either Na^+ or Mg^{2+} ions, or both, were added to neutralize the complex systems. In one case the NMR structure was neutralized by 37 Na^{2+} ions and in the other by 18 Mg^{2+} ions and one Na^+ ion. The structure determined by X-ray diffraction was neutralized either with Na^+ or Mg^{2+} ions (22 and 11 of them, respectively). The solvated complexes were geometry optimized using the steepest descent and conjugate gradient methods, 2500 steps of each. After optimization, systems were equilibrated for 0.6 ns in three steps. During each of the 0.2 ns long step temperature increased for 100 K. The equilibrated systems were subjected to 70 ns of productive, unconstrained molecular dynamics (MD) simulations at constant temperature and pressure (300 K, 1 atm). The time step during the simulations was 1 fs and the temperature was held constant by using Langevin dynamics with a collision frequency of 1 ps^{-1}. Geometry optimization and molecular dynamic simulations were performed using the AMBER12[27] program pmemd. The simulations were performed using periodic boundary conditions (PBC). The long range electrostatic interactions were calculated by the Particle Mesh Ewald (PME) method using the cutoff distance of 11 Å for the pairwise interactions in the direct space.

The trajectories were visualized using the VMD 1.8.7 program. MD trajectories manipulation and analysis were performed by Ptraj program available within the AMBER12Tools. The polynucleotide chain bending was traced by angle between three P atoms from residues 49, 56 and 65 (Fig. 2).

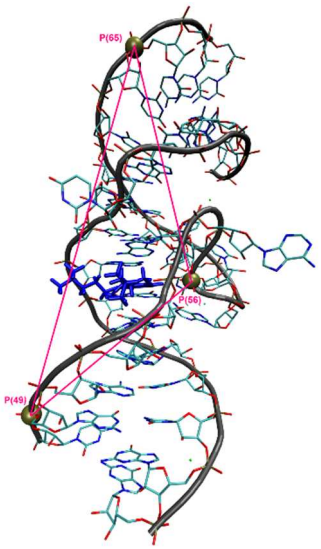

Fig. 2 Definition of "3P-angle" used in analysis of the polynucleotide shape.

The binding free energies were calculated using the Molecular Mechanics Poisson-Boltzmann Surface Area (MM-PBSA)[28] approach as implemented in the AMBER10[29] program. The calculations were performed on 80 snapshots, sampled during the last 4 ns of the productive MD simulations, using the equation:

$$\Delta G_{bind} = G_{complex} - \left(G_{receptor} + G_{ligand}\right).$$

The Gibbs free energies were approximated with the sum of conformational energy and the free energy of solvation. The polar component of the solvation free energy was calculated using the Poisson-Boltzmann method and the non-polar component was evaluated according to the equation:

$$\Delta G_{non-polar} = \gamma SASA + \beta ,$$

in which the solvent-accessible surface area (SASA) was calculated using MolSurf program.[30] The surface tension γ and the offset β were set to the standard values of 0.00542 kcal/(molÅ^2) and 0.92 kcal/mol, respectively. The entropic contribution to the binding free energy was approximated with the vibrational contribution calculated using NMode modul available within the AMBER10.[29]

Influence of the environment on the charge distribution at ligands (**2** and **3**) was determined using quantum mechanical (QM) and the ONIOM QM/MM methods. Calculations were performed by the program Gaussian09.[23] The QM/MM calculations were performed in the gas phase with and without the presence of magnesium ions. Within this approach ligand was treated quantum mechanically ("QM" region) and the rest of the system, RNA and ions ("MM" region), empirically using the AMBER force field ff99.[31] The QM calculations were performed using DFT (B3LYP/6-31G) method. The electrostatic interactions between "QM" and "MM" regions were studied using mechanical embedding (ME) and electrostatic embedding (EE). QM studies of ligands, **2** and **3**, in an polarisable environment were performed at the same level of theory (B3LYP/6-31G) using polarizable continuum model (PCM),[32] with dielectric constant of 78.39.

Results and discussion

In order to study influence of environment, mutations and ligands on the three-dimensional structure, flexibility and stability of the IRES subdomain IIa we constructed 12 different systems (see Table S1 in ESI†) and subjected them to the 70 ns long MD simulations.

Molecular dynamic simulations of the IIa RNA subdomain

Investigation of the plasticity of the ligand-free form of the subdomain IIa was performed using the structures determined by two experimentally different techniques, X-ray diffraction and NMR (PDB codes 3TZR and 2KTZ, respectively; for details see section Material and methods) as initial. The inhibitor **2**, which is part of both structures, was removed and the RNAs were simulated in and without the presence of the magnesium ions. During 70 ns of the productive MD simulations, all free, unliganded structures slightly folded, except the NMR structure (Table S1 in ESI†). Apparently the

Mg^{2+} ions are required for stabilization of RNA in the active, L-shaped, form. During simulations with magnesium ions RNA folded more, in the case of NMR structure significantly, and in the case of X-ray structure, slightly, than when in simulations with sodium ions only. The angle defined by phosphorus atoms, at nucleotides 49, 56 and 65, which span the full RNA length, "3P-angle", (Fig. 2) was used as a measure of the RNA bending. During simulation with the Mg^{2+} ions included, both unliganded IIa structures, 'X-ray' and 'NMR', changed their conformation from the extended to the bended one, and "3P-angle" decreased for approximately 30 degrees. The 'NMR' structure reached it's the most compact form after approximately 46 ns of MD simulations with "3P-angle" approximately 66 degrees smaller than in the initial structure (Fig. 3). During subsequent simulations the RNA slightly extended, and after 70 ns of productive simulations, the "3P-angle" was approximately 30 degrees smaller than in the initial structure (see Figs. S1 and S2 in ESI†). Although a deep cavity in RNA structures induced by ligand binding, restructured during MD simulations of the unliganded polynucleotides the Mg^{2+} ions bound in the vicinity of nucleotides G110, A53 and G52 only slightly changed their position.

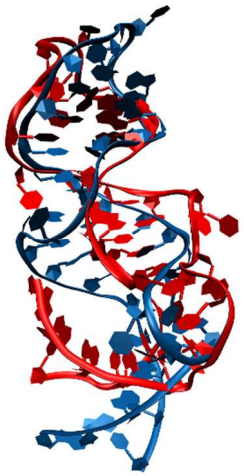

Fig. 3 Alignment of IIa structure before (blue), and after (red) 46 ns of MD simulation. The initial structure is the one determined by NMR for RNA complexed with **2**.

According to the MM-PBSA calculations the conformational enthalpy decreased upon the RNA bending (see Tables S2-S4 in ESI†). Namely, the free energy of the initially extended IIa conformation is about 36 kcal/mol higher than the energy of the L-shaped structure obtained by MD simulations (see Table S4 in ESI†).

Molecular dynamic simulations of the complexes with the benzimidazole ligands

In order to determine influence of ligands and mutations on the RNA structure, as well as to elucidate details of interactions between the IRES subdomain IIa and its ligands: DAP, **6**, and the benzimidazole inhibitors **2** (*R* and *S* enantiomer) and **1** and the analogue **3** (Fig. 1) we performed a detailed molecular modelling simulations study. Besides the native IIa subdomain complexes (with **1**, **2**, **3**, and **6**) we also simulated the complexes between two double mutants of IIa and the inhibitor **2**. According to the *crystallographically* determined structure, guanine G110 is hydrogen bonded to the inhibitor **2**, so, by study of the complexes between mutated RNA and **2** we wanted to get clue about importance of this interaction. All benzimidazole ligands remind tightly bound into the subdomain IIa RNA ligand-binding pocket during entire, 70 ns long, MD simulations. However, while the inhibitors (**1** and **2**) were intercalated between two parallel, neighbouring, bases, guanine G52 and adenine A53, as shown in Fig. 4 and Fig. S3 in ESI†, during simulations of the IIa–**3** complex A53 flipped and the base parallelism was lost, see Fig. S4 in ESI†. The three magnesium ions located in ligand-binding site and contributing to the stabilization of the bonded ligand also remained close to their initial positions during the simulations of all complexes with the benzimidazole ligands. However, the RNA shape changed in different ways during the simulations (see Figs. 5-7 and Fig. S5 in ESI†). During simulations of the RNA complex with inhibitors **1** and **2** the subdomain IIa (Fig. 5) even more stretched, and the "3P-angle" (Fig. 2) increased for approximately 10 - 25 degrees (Fig. 6). The structure of the subdomain IIa RNA target in complex with the benzimidazole analogue **3** was built in the same way as with the inhibitor **1**, by replacing **2** in the 'X-ray' structure of the complex. However, during MD simulations of the IIa–**3** complex the subdomain IIa, differently than in the complexes with the benzimidazole inhibitors, bended, and the "3P-angle" decreased approximately 30 degrees (Figs. 6 and 7). The noticed conformational changes of IIa in the complexes with the benzimidazole ligands is in agreement with the experimental (FRET) measurements of Dibrov et al.[17] and support their assumption about the mechanism by which the benzimidazole compounds **1** and **2** inhibit HCV replication. Inability of the benzimidazole ligand **3** to lock the subdomain IIa in an extended conformation, what very efficiently did **1** and **2**, explains why it is not a good HCV inhibitor. Namely, in order to be functional the IRES subdomain IIa should be able to adopt L-shape and after the interaction with ribosome, to switch from the bended to an extended shape. However, from these simulations it was not clear whether benzimidazole inhibitors could induce transformation of IIa from the bended to extended conformation (or they only stabilize stretched form of IIa). To check whether the benzimidazole inhibitors could induce straightening of the subdomain IIa we simulated complexes between folded (L-shaped) IIa and **2** (see Materials and methods for details). During the MD simulations, the L-formed structure of IIa extended and the "3P-angle" increased for approximately 40 degrees (Fig. S2 in ESI†).

According to the results of MM-PBSA binding free energy calculations the complex with the inhibitor **2** is the most stable, follows complexes with **1**, of comparable stability, and with **3**, significantly less stable, (see Table S5 in ESI†). During simulations the inhibitor **2** was stabilized by five intermolecular hydrogen bonds (see the structure obtained after 70 ns of MD simulations shown in Fig. 4). Two of them were established

between the benzimidazole inhibitor NH_2 group and the neighbouring nucleotide at position 110, with the base, guanine, and with the backbone phosphate group. The same phosphate group hydrogen bonded to the protonated dimethylamino-propyl side chain of the ligand. The fourth hydrogen bond was formed between the NH^+ group from benzimidazole ring and the neighbouring G110, carbonyl oxygen, and the fifth one was between the second protonated dimethylamino-propyl side chain of the ligand and the G52 phosphate group. The intermolecular hydrogen bonds between **2** and the neighbouring guanine G110 (the hydrogen bonds labelled 3 and 4 in Fig. 4) participate in Hoogsteen edge recognition of G110-C58 base pair by benzimidazole **2**.

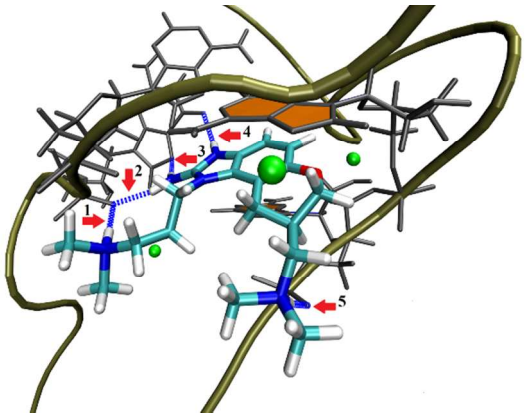

Fig. 4 The ligand binding site (after 70 ns of MD simulations). Inhibitor **2** is intercalated between two bases (above A53, below G52, shown in orange). Mg^{2+} ions are shown in green. Intermolecular hydrogen bonds formed between: 1) HN(**2**)-O2P(G110), 2) H031(**2**)-O2P(G110), 3) H032(**2**)-N7(G110), 4) H01(**2**)-O6(G110) and 5) H04(**2**)-O1P(G52) are shown as blue dashed lines and indicated by red arrows.

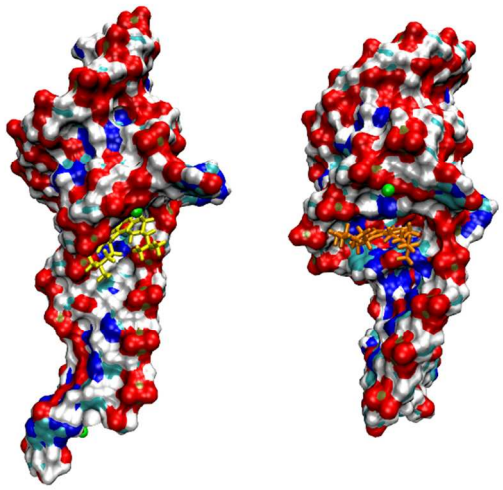

Fig. 5 Left: the final, optimized structure of the complexes between IIa and inhibitors **2** (yellow) and **1** (orange), shown left and right, respectively.

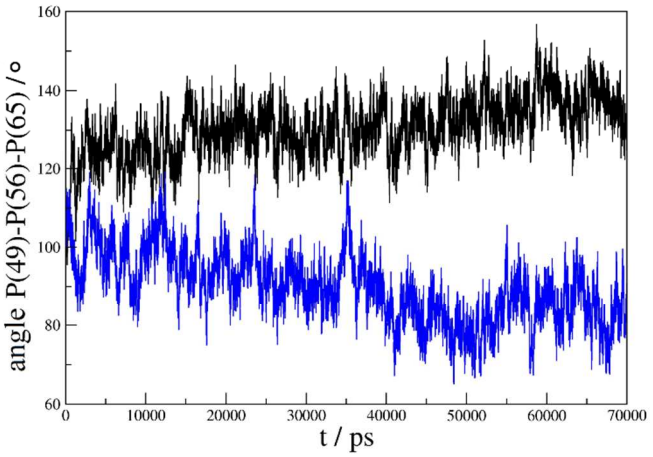

Fig. 6 Comparison of "3P-angle" changes during MD simulations of the IIa complexed with inhibitor **2** (black) and analogue **3** (blue), respectively.

The inhibitor **1** was, besides by the stacking π-π interaction, stabilized by three intermolecular hydrogen bonds during MD simulations. One hydrogen bond was established between the NH group from the protonated dimethylamino-propyl side chain and the neighbouring RNA backbone phosphate group at A109 and the other two bonds were formed with the neighbouring guanine G110, HN03(**1**)-N7(G110) and H01(**1**)-O6(G110), (Fig. S3 in ESI†). The time dependent plots of the inhibitor(s) - RNA hydrogen bond distances (sampled during 70 ns long MD simulations) are displayed in the ESI† Fig. S6. In comparison with the inhibitor **2**, analogue **3**, is lacking two protein donors. Consequently its stabilization within the binding pocket was less efficient. Namely, it was stabilized with two hydrogen bonds both with the neighbouring guanine G110. One was established with the NH^+ group from the benzimidazole ring and the other with the protonated dimethylamino-propyl side chain of the analogue (Fig. S4 in ESI†). Besides, as already mentioned the parallelism with the neighbouring bases was disrupted during MD simulation of the complex with the analogue, and as a consequence the stacking π-π interaction was weakened.

The complexes of the benzimidazole inhibitor **2** with the subdomain IIa double mutants I and II were built by replacing the binding site guanine, G110, either by cytosine or adenine, respectively, whereas the Watson-Crick pairing was retained (see Materials and methods for details). In the complexes with the IIa mutants **2** remained intercalated between bases A53 and G52, like in the complex with native IIa, during MD simulations. However, the hydrogen bonds between the benzimidazole inhibitor and the base at position 110 have not been established during simulations. In agreement with the reduced number of hydrogen bonds in the mutated complexes, the MM-PBSA calculations revealed that binding affinity of the inhibitor **2** toward mutated RNAs significantly decreased, in comparison with the affinity toward the native IIa (see Table S5 in ESI†). Apparently, G110 is key base for the benzimidazole inhibitors stabilization.

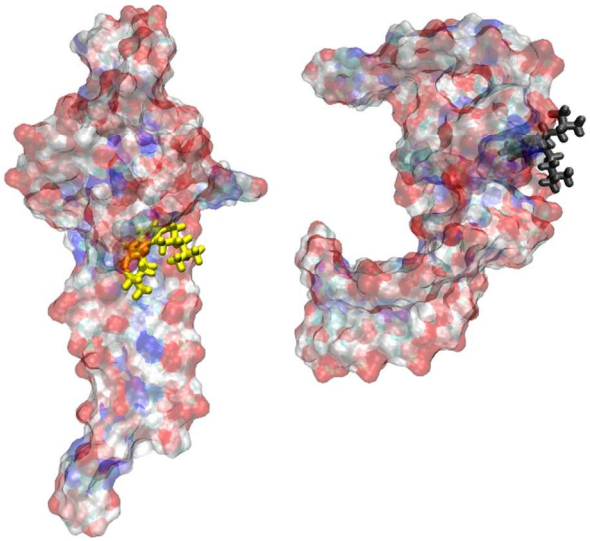

Fig. 7 Results of MD simulations of the subdomain IIa complexed with **2** (shown in yellow), left, and **3** (shown in grey), right.

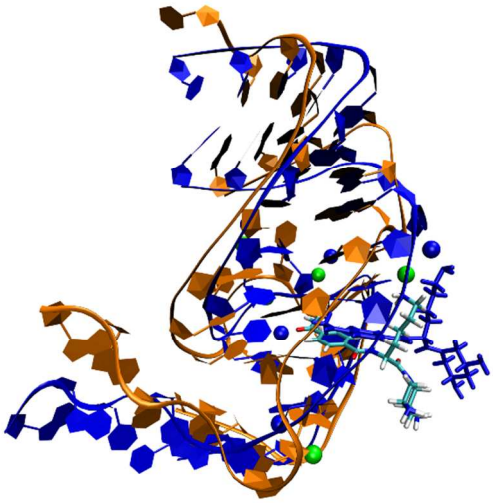

Fig. 8 The initial (blue) and final, obtained after 70 ns of MD simulations and optimised, structure of the IIa–DAP **6** complex ("bm1").

Molecular dynamic simulations of the subdomain IIa complexed with DAP 6

Since the experimentally determined structure of the IIa–DAP **6** complex was not available nor were data about the ligand interactions with RNA we built three different complexes using the bent form of the IIa (the one obtained by MD simulations). In two of them, ("bm1" and "bm2") phenyl methyl ketone was intercalated and the rest of the molecule was placed in the RNA minor groove (for details see Materials and methods). In the both complexes DAP remained intercalated during the simulations. However, while in the case of "bm1" the RNA form was preserved during MD simulations (Fig. 8) in the complex with the diaminopiperidine part of the molecule pointing to the opposite RNA and the L-shaped form of the IIa was disturbed (not shown). The complex with DAP bound into the RNA minor groove disintegrated during the simulation i.e. the ligand left the RNA minor groove. The simulation results suggest that DAP binds to IIa as an intercalator, which is consistent with the assumption of Dibrov et al.[19] According to the binding free energy calculations the "bm1" binding mode is more stable than "bm2" (Table S6 in ESI†). Further, in the previous complex RNA remained L-shaped during MD simulations consistently with the experimental results which suggested that DAP locks the IIa RNA switch in the bent conformation.

QM and QM/MM calculations – how binding to RNA influences the charge distribution at benzimidazole ligands.

In order to determine in what extent the RNA subdomain IIa and Mg^{2+} ions influence the benzimidazole ligands and to find out whether we could correlate the intensity of the charge distribution variations with the binding affinity, QM and QM/MM calculations were performed for inhibitor **2** and analogue **3** at different environments. For this purpose we have used the optimised structures of the complexes obtained from MD simulations.

The QM calculations were performed in the polarisable environment that mimicked water while the complexes with RNA were studied using the hybrid, QM/MM approach. The ESP charges calculated for the ligands in different environment are summarized in Tables S7 and S8 (ESI†). As expected, the largest variations of the charge distribution was noticed at atoms that upon ligand binding intercalated between the neighbouring RNA bases and became completely desolvated, see Fig. 9. It was found that, both, the charge distribution and the ONIOM energies were significantly affected by the presence of Mg^{2+} ions placed close to the ligand binding site (Table S9 in ESI†). Apparently the magnesium ions play an important role in stabilization of the complexes between IIa RNA and benzimidazole ligand **2** in an extended conformation. Larger stability of the RNA complex with the **2** than with **3** is in agreement with the experimentally measured $EC6_{50}$[17] and correlate with the (ca 20%) larger variation of atomic charges on the inhibitor, **2**, than on analogue, **3**.

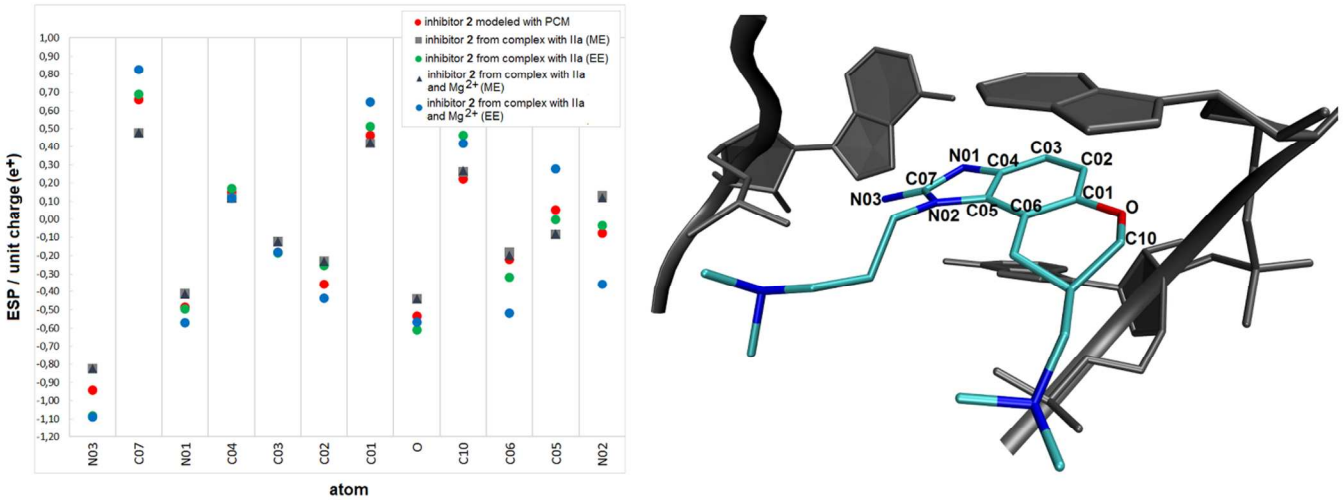

Fig. 9 Influence of the RNA environment on the ligand charge distribution. Left: the ESP charges, at the selected inhibitor atoms, determined in different environments. Right: the ligand binding site with the atoms, that experience the largest polarization, labelled. For the details of the RNA - inhibitor **2** interactions (H-bonds and interactions with Mg^{2+}) see Fig. 4. The ligand orientations in Figs 4 and 9 are identical.

Conclusions

In this work plasticity and stability of the IRES subdomain IIa were studied using molecular modelling methods. The obtained results suggest that conformational changes of IIa are reversible indicating. According to MD simulations benzimidazole inhibitors move stability of the subdomain IIa toward an extended conformation while the diaminopiperidine derivative **6** stabilizes the bent, L-shaped, form of IIa. Besides, it was shown that the benzimidazole inhibitor **2** could induce transformation of IIa from the bended to an extended shape. Combined QM and QM/MM calculations revealed correlation between the binding affinities and the degree of variation of the ligand charge distribution upon binding.

Acknowledgements

We thank the Ministry of Science, Education and Sport of the Republic of Croatia for financial support (grant no. 098-1191344-2860), the Croatian National Grid Infrastructure (CRO NGI)[33] and Isabella computing cluster.[34]

Notes and references

[a] Laboratory for Chemical and Biological Crystallography, Division of Physical Chemistry, Ruđer Bošković Institute, HR 10002 Zagreb, P.O.B. 180, Croatia. E-mail: tomic@irb.hr

† Electronic Supplementary Information (ESI) available. See DOI: 10.1039/b000000x/

1 D. Lavanchy, Clin. Microbiol. Infect., 2011, **17**, 107-115.
2 M. Enserink, Science, 2011, **332**, 159-160.
3 P. Y. Wang, B. K. Chun, S. Rachakonda, J. F. Du, N. Khan, J. X. Shi, W. Stee, D. Cleary, B. S. Ross and M. J. Sofia, J. Org. Chem., 2009, **74**, 6819-6824.
4 J. J. Feld and J. H. Hoofnagle, Nature, 2005, **436**, 967-972.
5 S. Kota, V. Takahashi, F. Ni, J. K. Snyder and A. D. Strosberg, PLoS One, 2012, 7.
6 M. Robinson, Y. Tian, W. E. t. Delaney and A. E. Greenstein, Proc. Natl. Acad. Sci. U. S. A., 2011, **108**, 10290-10295.
7 C. U. Hellen, Biochim. Biophys. Acta, 2009, **1789**, 558-570.
8 D. R. Davis and P. P. Seth, Antivir. Chem. Chemother., 2011, **21**, 117-128.
9 J. S. Kieft, K. Zhou, R. Jubin, M. G. Murray, J. Y. Lau and J. A. Doudna, J Mol Biol, 1999, **292**, 513-529.
10 M. Honda, M. R. Beard, L. H. Ping and S. M. Lemon, J. Virol., 1999, **73**, 1165-1174.
11 J. S. Kieft, K. Zhou, R. Jubin and J. A. Doudna, RNA, 2001, **7**, 194-206.
12 C. M. Spahn, J. S. Kieft, R. A. Grassucci, P. A. Penczek, K. Zhou, J. A. Doudna and J. Frank, Science, 2001, **291**, 1959-1962.
13 D. Boehringer, R. Thermann, A. Ostareck-Lederer, J. D. Lewis and H. Stark, Structure, 2005, **13**, 1695-1706.
14 P. J. Lukavsky, I. Kim, G. A. Otto and J. D. Puglisi, Nat. Struct. Biol., 2003, **10**, 1033-1038.
15 S. M. Dibrov, H. Johnston-Cox, Y. H. Weng and T. Hermann, Angewandte Chemie, 2007, **46**, 226-229.
16 M. E. Filbin and J. S. Kieft, RNA, 2011, **17**, 1258-1273.
17 S. M. Dibrov, K. Ding, N. D. Brunn, M. A. Parker, B. M. Bergdahl, D. L. Wyles and T. Hermann, Proc. Natl. Acad. Sci. USA, 2012, **109**, 5223-5228.
18 R. B. Paulsen, P. P. Seth, E. E. Swayze, R. H. Griffey, J. J. Skalicky, T. E. Cheatham, 3rd and D. R. Davis, Proc. Natl. Acad. Sci. U. S. A., 2010, **107**, 7263-7268.
19 S. M. Dibrov, J. Parsons, M. Carnevali, S. Zhou, K. D. Rynearson, K. Ding, E. Garcia Sega, N. D. Brunn, M. A. Boerneke, M. P. Castaldi and T. Hermann, J. Med. Chem., 2014, **57**, 1694-1707..

20 http://accelrys.com/services/training/life-science/insight-migration.html.
21 W. D. Cornell, P. Cieplak, C. I. Bayly, I. R. Gould, K. M. Merz, D. M. Ferguson, D. C. Spellmeyer, T. Fox, J. W. Caldwell and P. A. Kollman, J Am Chem Soc, 1995, **117**, 5179-5197.
22 Y. Duan, C. Wu, S. Chowdhury, M. C. Lee, G. M. Xiong, W. Zhang, R. Yang, P. Cieplak, R. Luo, T. Lee, J. Caldwell, J. M. Wang and P. Kollman, J Comput Chem, 2003, **24**, 1999-2012.
23 M. J. Frisch, G. W. Trucks, H. B. Schlegel, G. E. Scuseria, M. A. Robb, J. R. Cheeseman, G. Scalmani, V. Barone, B. Mennucci, G. A. Petersson, H. Nakatsuji, M. Caricato, X. Li, H. P. Hratchian, A. F. Izmaylov, J. Bloino, G. Zheng, J. L. Sonnenberg, M. Hada, M. Ehara, K. Toyota, R. Fukuda, J. Hasegawa, M. Ishida, T. Nakajima, Y. Honda, O. Kitao, H. Nakai, T. Vreven, J. A. Montgomery, Jr., J. E. Peralta, F. Ogliaro, M. Bearpark, J. J. Heyd, E. Brothers, K. N. Kudin, V. N. Staroverov, R. Kobayashi, J. Normand, K. Raghavachari, A. Rendell, J. C. Burant, S. S. Iyengar, J. Tomasi, M. Cossi, N. Rega, N. J. Millam, M. Klene, J. E. Knox, J. B. Cross, V. Bakken, C. Adamo, J. Jaramillo, R. Gomperts, R. E. Stratmann, O. Yazyev, A. J. Austin, R. Cammi, C. Pomelli, J. W. Ochterski, R. L. Martin, K. Morokuma, V. G. Zakrzewski, G. A. Voth, P. Salvador, J. J. Dannenberg, S. Dapprich, A. D. Daniels, Ö. Farkas, J. B. Foresman, J. V. Ortiz, J. Cioslowski and D. J. Fox, Gaussian, Inc., Wallingford CT, 2009.
24 A. D. Becke, J Chem Phys, 1993, **98**, 5648-5652.
25 K. D. Dobbs and W. J. Hehre, J Comput Chem, 1987, **8**, 880-893.
26 D. A. Case, Darden, T. A., Cheatham III, T. E., Simmerling, C. L., Wang, J., Duke, R. E., Luo, R., Walker, R.C., Zhang, W., Merz, K. M., Roberts, B., Wang, B., Hayik, S., Roitberg, A., Seabra, G., Kolossváry, I., Wong, K. F., Paesani, F., Vanicek, J., Liu, J., Wu, X., Brozell, S. R., Steinbrecher, T., Gohlke, H., Cai, Q., Ye, X., Wang, J., Hsieh, M.-J., Cui, G., Roe, D. R., Mathews, D. H., Seetin, M- G., Sagui, C., Babin, V., Luchko, T., Gusarov, S., Kovalenko, A., Kollman, P. A. , University of California, San Francisco, 2010.
27 D. A. Case, T. A. Darden, I. T.E. Cheatham, C. L. Simmerling, J. Wang, R. E. Duke, R. Luo, R. C. Walker, W. Zhang, K. M. Merz, B. Roberts, S. Hayik, A. Roitberg, G. Seabra, J. Swails, A. W. Götz, I. Kolossváry, K. F. Wong, F. Paesani, J. Vanicek, R. M. Wolf, J. Liu, X. Wu, S. R. Brozell, T. Steinbrecher, H. Gohlke, Q. Cai, X. Ye, J. Wang, M.-J. Hsieh, G. Cui, D. R. Roe, D. H. Mathews, M. G. Seetin, R. Salomon-Ferrer, C. Sagui, V. Babin, T. Luchko, S. Gusarov, A. Kovalenko and A. Kollman, University of California, San Francisco, 2012.
28 J. M. J. Swanson, R. H. Henchman and J. A. McCammon, Biophys. J., 2004, **86**, 67-74.
29 D. A. Case, T. A. Darden, T. E. Cheatham III, C. L. Simmerling, J. Wang, R. E. Duke, R. Luo, M. Crowley, R. C. Walker, W. Zhang, K. M. Merz, B. Wang, S. Hayik, A. Roitberg, G. Seabra, I. Kolossváry, K. F. Wong, F. Paesani, J. Vanicek, X. Wu, S. R. Brozell, T. Steinbrecher, H. Gohlke, L. Yang, C. Tan, J. Mongan, V. Hornak, G. Cui, D. H. Mathews, M. G. Seetin, C. Sagui, V. Babin and P. A. Kollman, University of California, San Francisco, 2008.
30 M. L. Connolly, J. Appl. Crystallogr., 1983, **16**, 548-558.
31 J. M. Wang, P. Cieplak and P. A. Kollman, J Comput Chem, 2000, **21**, 1049-1074.
32 S. Miertus, E. Scrocco and J. Tomasi, Chem Phys, 1981, **55**, 117-129.
33 http://www.cro-ngi.hr/
34 http://www.srce.unizg.hr/studenti/napredno-racunarstvo/racunalni-klaster-isabella/